Received February 1, 2013, accepted May 13, 2013, date of publication May 30, 2013, date of current version June 13, 2013.

Digital Object Identifier 10.1109/ACCESS.2013.2265551

Plasmonics in Nanoslit for Manipulation of Light

TAERIN CHUNG, SEUNG-YEOL LEE, HANSIK YUN, SEONG-WOO CHO, YONGJUN LIM, IL-MIN LEE, AND BYOUNGHO LEE (Senior Member, IEEE)

National Creative Research Center for Active Plasmonics Application Systems, Inter-University Semiconductor Research Center and School of Electrical Engineering, Seoul National University, Seoul 151-744, Korea

Corresponding author: B. Lee (byoungho@snu.ac.kr)

This work was supported by the National Research Foundation of Korea through the Creative Research Initiatives Program (Active Plasmonics Application Systems).

ABSTRACT A nanoslit is capable of performing versatile functions in nanophotonic applications. In this invited paper, we discuss the physics and manipulation methods of surface plasmon excitation such as directional switching at a nanoslit. Furthermore, enhancing the light intensity passing through a nanoslit by employing embedded metallic nanoislands is experimentally presented and numerically analyzed.

INDEX TERMS Surface plasmon, plasmonics, nanostructures, subwavelength slit.

I. INTRODUCTION

Recent years have seen a major footstep of research into nano-photonics based on surface plasmon polaritons (SPPs). SPPs are optical-frequency or terahertz electromagnetic waves coupled with collective oscillation of electron plasma in metal [1]. SPPs can be excited under appropriate condition when the light or terahertz wave is incident on the interface between dielectric and the noble metal that has the negative real part of permittivity. They propagate along or become trapped at metal-dielectric interfaces. Electromagnetic waves can be fumbled with metallic nanostructures beyond the diffraction limit with the help of SPPs. For example, various types of metallic nanostructure have been proposed for guiding SPP modes. These contain thin metal film [2]–[4], chains of metal nanoparticles [5]–[7], various shapes of metal nanorods [8]–[10], and nanoholes in a metallic medium [11]–[14], nanogaps between metallic media, and slot waveguides in the form of rectangular nanogaps in thin metal film [15]–[18]. Metallic nanostructures can also convert optical radiation into intense, engineered, localized plasmonic field distribution, functioning as plasmonic antennas and lenses [19], [20]. Thus, wherever subwavelength control over light is desired, metallic nanostructures are likely to act as a tangible part. Hence many researches relevant to a subwavelength metallic slit in optical regime have been endeavored for overcoming the diffraction limit [21]–[24]. Studies on plasmonic beaming [25], [26] and focusing phenomena [27], [28] are some of the key issues in this research field. Furthermore, a nanoscale metallic slit, also called ''nanoslit'', has received much attention and been utilized in wide ranges of plasmonics [29]. A nanoslit can play versatile roles for plasmonic circuits, nano-resolution optical imaging techniques and sensors. It acts as a plasmonic waveguide which transmits the light into confined region. It can also function like a plasmonic antenna so that it enhances near-field intensity or far-field radiation.

In this invited paper, we briefly review on the fundamentals of a nanoslit and provide extended researches that involve the SPP excitation mechanism at a nanoslit. These results will be mainly discussed in Section II. In addition, we propose and experimentally demonstrate the new pathway to enhance light intensity passing through a nanoslit by the use of embedded metallic nanoislands via far-field scattering microscopy. Numerical analysis to support experimental results is offered, which will be investigated in Section III.

II. THE USE OF NANOSLIT FOR MANIPULATION OF SURFACE PLASMON EXCITATION

A. BRIEF REVIEW ON ISSUES OF PLASMONICS IN NANOSLIT

A nanoslit can play distinctive roles in plasmonics. Not only did light fields simply transmit, but also they could enhance field intensity [30]–[32] or control field distribution [33]. Especially, significant near-field enhancement has been mostly observed in terahertz (THz) region. In this frequency region, it is possible to make a size of nanoslit much smaller than the incident wavelength. It has been shown that about the degree of three orders in field enhancement factor could be observed from an extremely narrow subwavelength slit

TABLE 1. Representative Works on Plasmonics in Nanoslit

Geometry	Purpose	FE factor	Freq. (THz)	Ref
Single nanoslit	Field enhancement	~1000	0.1–1.1	[30]
		~20	0.2–2.0	[31]
		~5	474	[32]
	Directional launching & switching	-	564	[43]
		-	564	[44]
Nanoslit array	Field enhancement	~1000	0.01–1	[45]
		~760	0.2–2.7	[46]
		~10	333–750	[36]
	Nearly perfect transmission	~5	0.01–2	[40]
		-	0.2–21.4	[47]
		~5	55–120	[35]
	Optical sensing	-	300–450	[48]
Nanoslit with gratings	Field enhancement	~10	375	[37]
		~3.2	300–900	[38]
		~7	333–750	[39]

Note that the measured location of field enhancement factor can be different from each other.

whose dimension is approximated by λ/30,000 of slit width [30]. Since the size of a nanoslit is quite smaller than THz wavelength, the physical aspects have been often modeled with quasi-static approximations of surface currents induced by external sources; the nanoslit can be modeled as local capacitor [34]. However, as the operating wavelength becomes shorter, two major effects are taken account of the models that are adopted in terahertz region: one is the plasmonic effect, whereas the other is the quantum effect. Plasmonic effects can give rise to additional near-field enhancement or the increase of transmitted light intensity [32], [35]. Extraordinary optical transmission or absorption in optical frequency is one of the representative phenomena arisen from plasmonic effects [11], [32]. Moreover, various structures such as tapered-shape of nanoslits [36], the nanoslit supported by gratings [37]–[39], and nanoslit arrays [40] have been employed to enhance the plasmonic effects for the purpose of field enhancement in optical region.

On the other hand, quantum effects mostly give a limitation of field enhancement in a nanoslit. In addition to the difficulty to fabricate the nanoslit far narrower than optical wavelength for experimental demonstration, recent reports tell us that enormous field enhancement observed in terahertz region cannot be applied to sub-nano scale structures in both theory and experiment due to the quantum effects including nonlocal effects in the optical properties of metal [41] and quantum tunneling [42]. Very recently, these quantum aspects on an extremely narrow gap have been experimentally demonstrated by nearly connecting two atomic force microscopes [42].

As we discussed above, diverse topics and comprehensive issues associated with nanoslit (or nanogap) have been addressed throughout broad wavelength region from terahertz to visible region. It is difficult to summarize all of them because the purposes and applications of these works are quite diverse. Thus, we categorize some of distinguished works done with nanoslit geometries in Table 1 [30]–[32], [35]–[40], [43]–[48], accompanying with functional description for brief summarization. In Table 1, reported maximum field enhancement factors are summarized for the each case. For the convenience of comparing results, we provide field enhancement factor values based on the enhancement of field amplitude.

B. BASIC PRINCIPLES ON A NANOSLIT: MODE ANALYSIS IN METAL-INSULATOR-METAL WAVEGUIDE

According to the studies that have used a nanoslit for the excitation source of SPPs, a nanoslit can be naturally regarded as a plasmonic waveguide structure which transmits light into the confined region [49]–[52]. In this section, brief review on the modal analysis of metal-insulator-metal (MIM) plasmonic waveguide structures will be introduced to understand the underlying physics on SPPs excitation in a nanoslit geometry. At the finite length of a nanoslit, the edge effect of a nanoslit could distort the excited plasmon source from the ideal case of infinite length of a nanoslit. However, this is often negligible when the length of the nanoslit is quite longer than the slit width. Hence, in this section we will consider the infinite length of slit for theoretical investigations.

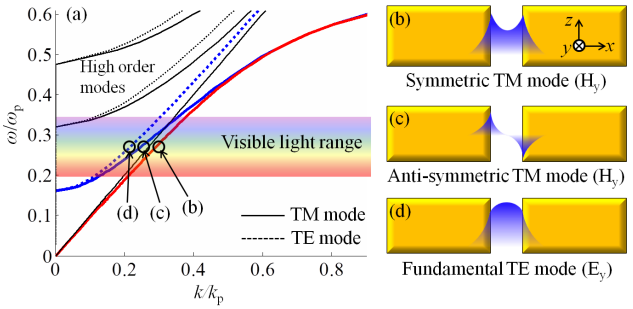

FIGURE 1. (a) Dispersion diagram of MIM plasmonic waveguide (slit in metal) with the 380 nm slit width is shown. Mode shapes of (b) symmetric plasmonic mode, (c) anti-symmetric plasmonic mode, and (d) fundamental TE photonic mode are illustrated. All solid and dotted lines indicate TM and TE modes regardless of their line colors, respectively.

For MIM waveguide, both of the transverse electric (TE) and transverse magnetic (TM) modes can exist as shown in Fig. 1, but only some of the TM modes can be called plasmonic modes due to their modal profiles [53]. In general, plasmonic mode is defined as a mode which has evanescently decaying modal profile both in the metal and insulator regions. Modes in MIM plasmonic waveguide can be calculated from the Maxwell's equations at the boundary of metal-insulator interfaces. For the symmetrical MIM waveguide, the dispersion relations of the layer system for TM mode can be

obtained as

$$TM : \begin{cases} \frac{\kappa_{x,metal}}{\varepsilon_{metal}} + \frac{\kappa_{x,air}}{\varepsilon_{air}} \tanh\left(\frac{\kappa_{x,air} w}{2}\right) = 0, \\ \frac{\kappa_{x,metal}}{\varepsilon_{metal}} + \frac{\kappa_{x,air}}{\varepsilon_{air}} \coth\left(\frac{\kappa_{x,air} w}{2}\right) = 0, \end{cases} \quad (1)$$

where κ_x, ε, and w denote the x-directional wavenumber, permittivity of the material, and the width of a nanoslit, respectively. Similarly, dispersion relations for TE mode can be expressed as

$$TE : \begin{cases} \frac{\kappa_{x,metal}}{\mu_{metal}} + \frac{\kappa_{x,air}}{\mu_{air}} \tanh\left(\frac{\kappa_{x,air} w}{2}\right) = 0, \\ \frac{\kappa_{x,metal}}{\mu_{metal}} + \frac{\kappa_{x,air}}{\mu_{air}} \coth\left(\frac{\kappa_{x,air} w}{2}\right) = 0. \end{cases} \quad (2)$$

In Fig. 1(a), dispersion curves of all modes existing in MIM plasmonic waveguide, which is composed of 380 nm air gap surrounded by silver layers, are illustrated. For the calculation of dispersion curves, we used Drude model for the permittivity of silver layer with the value of plasma frequency $\omega_p = 9eV$ and damping frequency $\gamma = 18\,meV$ [54]. It is well-known that the number of existing modes in MIM waveguide is significantly dependent on the ratio of incident wavelength to slit width. When the slit width is much narrower than the half of the incident wavelength, only the fundamental TM mode which has symmetric transverse magnetic field as shown in Fig. 1(b) can be observed. This mode is also often called fundamental plasmonic mode since the modal profile always evanescently decays both in the metal and insulator regions without mode cutoff, which means that the dispersion curve is always laid on the right side of the light line as shown in red solid line of Fig. 1(a). In the research field of plasmonics, this mode has received significant attention for chip-scale optical communications based on plasmonic waveguides because it does not have any cutoff frequency, so it would be possible to overcome the diffraction limit [55]. Moreover, this mode can be simply excited by normally illuminating the light into a nanoslit. Thus, it has been numerously applied to the design of plasmonic diffractive optics such as plasmonic beaming [25], focusing [27], vortex generation [56], [57], and sensing [58].

However, as shown in the Fig. 1(a), another plasmonic mode can simultaneously exist in the visible range of light in a nanoslit structure. Since this mode starts from the left side of the light line, it does not have evanescently decaying modal profile near the cutoff frequency. However, it is gradually changed from photonic to plasmonic modal profile and finally follows the dispersion curve of fundamental plasmonic mode. This secondary TM mode has anti-symmetric transverse magnetic field profile throughout the dispersion curve. It is often called anti-symmetric plasmonic or photonic mode. (In this invited paper, we call it anti-symmetric plasmonic mode.) Since this anti-symmetric plasmonic mode (Fig. 1(c)) has relatively poor confinement characteristics and difficult methodologies to launch SPP, not as much research is done for applying this mode into plasmonic devices. Although this mode may not be appropriate for transferring more energy into a subwavelength slit, recent works have shown that it can be utilized for the demonstration of directional switching of excited SPPs from a nanoslit [43], rainbow trapping due to their zero group velocity characteristics near the cutoff condition [59], and electro-optically modulated plasmonic modulators [60]. Furthermore, it is recently reported that the photonic TE mode, as illustrated in Fig. 1(d), which is always laid on the left side of light line and known as impossible to excite the SPPs since it does not have surface charge accumulation across the nanoslit for normal propagation, could be applied to the demonstration of polarization-dependent directional switching of SPPs from the nanoslit in the case of oblique propagation [44]. In the following sections, we will discuss on the methods for coupling the selective plasmonic mode in a nanoslit, and practical applications that use such slit-coupling characteristics for the manipulation of light such as directional guiding of SPPs, resonant frequency shifting, and enhancement of near- and far-field intensity by the use of embedded metallic nanoislands.

C. COUPLING CHARACTERISTICS OF SPPs IN A NANOSLIT FOR MANIPULATION OF LIGHT

As we discussed in previous section, a nanoslit can sustain several modes with totally different modal characteristics. Although all of these modes are the exact solutions of MIM layer system, each mode has specific coupling characteristics from incident light to the specific mode of MIM waveguide. Moreover, the out-coupling characteristics of each mode, which means the coupling amplitude and phase of excited SPPs propagating along the transmitted side of metal film, are also significantly different for case by case. For examples, it is known that only the TM modes can excite SPPs for normal incidence. Therefore, circularly polarized light can be attributed to amplitude modulation of excited surface plasmons, which brings an additional angular orbital number for circular-shaped plasmonic nanostructures [56], [61], [62]. Such characteristics have been often referred to as spin-orbital interaction. It is one of major issues in intensive research area of plasmonics. In addition, the phase symmetry of excited SPPs directly follows the field symmetry of the guided mode. These characteristics have been employed for generating plasmonic unidirectional couplings [43], [63]. Likewise, various recent works have tried to adopt the unique excitation mechanism of SPPs from a nanoslit in attempt to demonstrate plasmonic devices. Researchers also strive for revealing the physical origin of SPPs excitation mechanism in a nanoslit with the help of diverse models based on diffraction optics [64], [65], electromagnetic dipole [66] or induced surface charges [44]. These efforts to unveil the underlying physics on nanoslits have been devoted to modeling more complicate plasmonic structures such as nano-aperture [67], metamaterials [68], and plasmonic active devices [3].

In this section, we will explore the coupling characteristics of waveguide modes in a nanoslit according to the states of incident light such as polarization and incident momentum. Then we will briefly examine on the practical approach to control the direction of excited SPPs that are based on the out-coupling characteristics of guided plasmonic

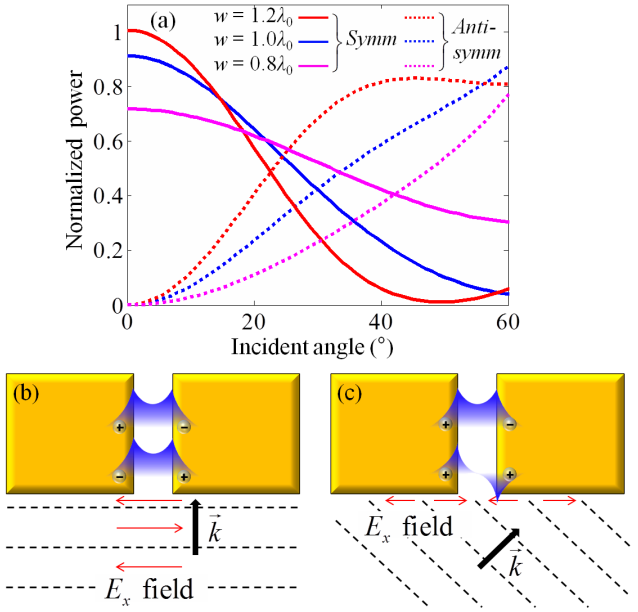

FIGURE 2. **(a) Coupling characteristics of plasmonic modes in Ag-air-Ag nanoslit at λ = 532 nm with the variation of incident angle and slit width are shown. Schematic diagrams for understanding the mode coupling mechanism on (b) normal and (c) oblique incidence cases.**

modes. First, we will investigate the coupling characteristics of plasmonic modes according to the linear momentum of incident light. In Fig. 2(a), we plotted the relative amount of coupled power from incident plane wave to symmetric (solid lines) and anti-symmetric (dotted lines) TM modes of half-infinite length of a nanoslit as a function of the incident angle, respectively. Here, the coupled power is normalized by the normal incidence case of $w = 1.2\,\lambda_0$ for symmetric TM mode (red solid line). As shown in Fig. 2(a), only the symmetric TM mode is generated for normal incidence case regardless of the value of slit width.

This can be easily understood by the parity of accumulated charge illustrated in Fig. 2(b). For normal TM incidence, electric field does not have lateral variation along the surface of metal film so that the directions of transverse electric field at the edges of a nanoslit are always same. Therefore, anti-symmetric plasmonic mode, which has opposite transverse electric fields, cannot be excited. On the other hand, it is shown that the amount of power coupled to anti-symmetric plasmonic mode is gradually increased as the incident angle becomes larger. In contrast, the amount of power coupled to symmetric plasmonic mode is decreased. This can also be understood from the parity of accumulated charges as shown in Fig. 2(c). In this case, transverse electric field changes its direction with the period of $\Lambda_x = \lambda_0/2\sin\theta_{inc}$. Therefore, opposite directions of electric fields are laid on each slit edge when the zero-field wavefront is located between the edges of nanoslit. Coupling efficiency to anti-symmetric plasmonic mode can be increased. In addition, it is shown that the increase of coupling power to anti-symmetric plasmonic mode becomes more rapid for wider slit width. The reason can also be explained by aforementioned analogy. It can be expected that zero-field wavefront is more frequently located between the slit edges when slit width is increased until Λ_x is similar to the value w.

Although it is hard to say the maximum coupling ratio is always directly related to the ratio of Λ_x to w due to the other effects such as the coupling from the longitudinal component of incident field which is dominant at the highly oblique incidence case, this relation between slit width and coupling ratio is well-depicted in Fig. 2(a). These characteristics for simultaneous excitation of symmetric and anti-symmetric modes have been utilized for asymmetric launching of surface plasmons [69].

However, it is shown that the conditions of a slit and incident angle to forbid coupling to symmetric plasmonic mode is quite restricted. To prevent the coupling to symmetric plasmonic mode for arbitrary slit conditions, it can be accepted to use an interference of two incident lights as shown in Fig. 3(a). Unlike the case of single oblique incidence, the node line of standing wave is not moving until the coherence of two sources is broken.

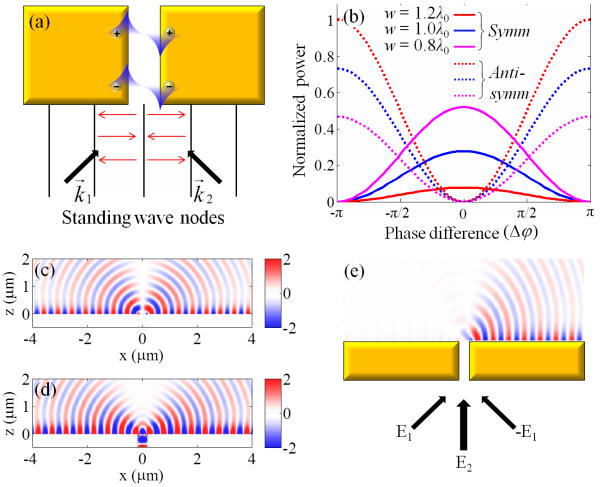

FIGURE 3. **(a) Schematic diagram for coupling mechanism with the interference pattern of two obliquely incident beams. (b) Coupling characteristics of plasmonic modes in nanoslit at λ = 532 nm with the variation of phase difference between two obliquely incident beams. The *z*−directional electric field profile on the transmission side of nanoslit with the incidence of (c) symmetric and (d) anti-symmetric plasmonic mode are shown. (e) Numerical results for unidirectional launching via three beam interference are reproduced [63].**

Therefore, accumulated surface charges at the edges of a nanoslit always have the same sign when the node line is exactly located at the center of a nanoslit. Only the anti-symmetric plasmonic mode can be excited. In Fig. 3(b), we plotted the coupled power to both modes as a function of phase difference between two incident waves. Here, we define the condition for zero phase difference ($\Delta\phi = 0$) when the

belly of standing wave is exactly located at the center of a nanoslit. As can be shown from the figure, only the anti-symmetric plasmonic mode is coupled from the interference pattern when the phase difference is $\Delta\phi = \pm\pi$ without regard to the slit width. Therefore, it may be quite simple to selectively control the amount of coupling ratio to each mode when the interference of two beams is used.

By using this selective mode launching scheme in a nanoslit structure, recent works demonstrated a surface plasmon directional switching by controlling the amount of coupled power to symmetric and anti-symmetric plasmonic modes [63]. In Figs. 3(c) and 3(d), the out-coupled z-directional electric fields from symmetric and anti-symmetric plasmonic modes are shown, respectively. Note that we illustrate longitudinal field component (E_z) with respect to a nanoslit rather than transverse one (E_x), to clearly show the propagating SPPs. It is shown that out-coupled SPPs from a nanoslit have anti-symmetric profile for symmetric MIM mode, whereas it has symmetric profile for anti-symmetric MIM mode. In Fig. 3(e), we reproduced a result for unidirectional launching with the method that was demonstrated in Ref. [63]. Here, two obliquely incident beams with opposite phases are used to excite the anti-symmetric mode, whereas normally incident beam is used for the excitation of symmetric mode. By controlling the relative amplitude and phase between oblique and normal incident beams, we can generate the SPPs unidirectionally for selective direction as shown in Fig. 3(e) by the interference of two types of SPPs.

As we discussed in Sub-section *A*, fundamental photonic TE mode has almost the same cutoff frequency with anti-symmetric plasmonic mode. A metallic slit which has two plasmonic modes has at least one photonic TE mode. Indeed, it is known that this mode cannot contribute to the generation of SPPs at a nanoslit especially for normal incidence case because this mode has only parallel-to-slit electric field component. However, it has been recently proved that the SPPs can also be excited from photonic TE mode when they obliquely propagate inside the metallic slit [44].

In Fig. 4(a), we illustrate the schematic diagram of incidence condition. Here, we assume half-infinite thickness of a nanoslit and regard that the incidence is given as an obliquely propagating specific mode with normalized amplitude. Since a nanoslit structure does not change the geometry along the y direction, y-directional momentum of incident light should be conserved. Therefore, the direction of out-coupled SPP wave has the relation of $\theta_{out} = \sin^{-1}(n_{MIM}\sin(\theta_{MIM})/n_{SPP})$, where n_{MIM} and n_{SPP} are effective indexes of MIM mode inside a nanoslit and out coupled surface plasmon mode, respectively.

In Fig. 4(b), the output coupling characteristics from photonic TE mode to surface plasmons are depicted with regard to the incident angle and slit width condition. It is shown that the coupling efficiencies are remarkably increased for higher incident angle condition. The physical origin in this aspect can be explained by the increase of oscillating

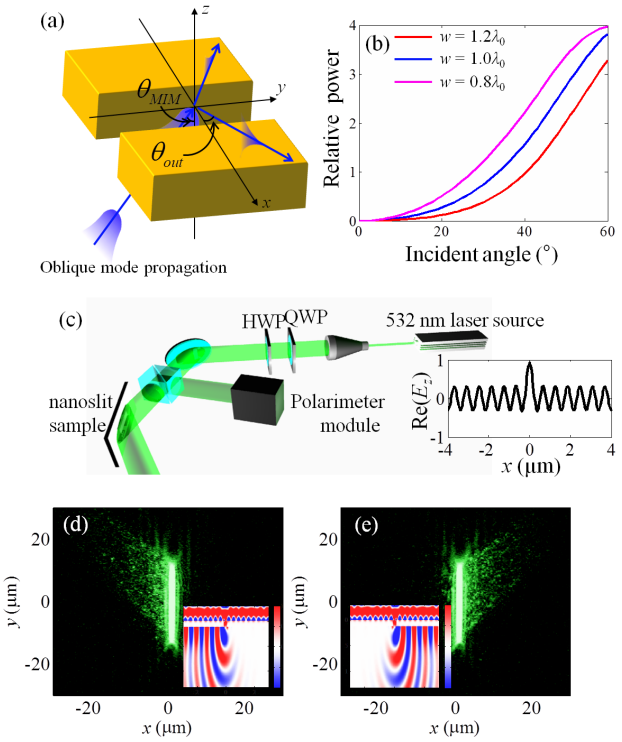

FIGURE 4. **(a) Schematic diagram for exciting the SPPs by obliquely propagating photonic TE mode is shown. (b) Out-coupling characteristics from photonic TE mode to excited SPPs at transmission side. (c) Experimental configuration for demonstrating polarization-modulated plasmonic switching is illustrated. (d)–(e) CCD images for polarization-modulated unidirectional launching are reprinted from the Ref. [44]. Copyright (2012) by the American Physical Society.**

induced charges near the slit edge, which is well-explained in Ref. [44]. In a similar manner as the case of anti-symmetric plasmonic mode, the phase profiles of out-coupled SPPs from oblique TE photonic mode are symmetric with respect to the center of a nanoslit as shown in the inset of Fig. 4(c). Hence, it also makes a switchable directional launching from a nanoslit by the interference of fundamental plasmonic (TM) mode and photonic (TE) mode. The significant difference of this achievement in comparison with the result in Fig. 3 is that the switching of SPP launching direction can be simply done by polarization modulation of single illumination as shown in the experimental setup illustrated in Fig. 4(c). In Figs. 4(d) and 4(e), results for polarization-modulated plasmonic switching are shown [44].

Throughout this section, we discussed about the coupling characteristics from incident waves to MIM modes in a nanoslit and excited SPPs at transmission side. We also reviewed on the methods of using these coupling characteristics for the manipulation of SPP excitations such as directional launching and plasmonic switching. In the next section, we will propose and discuss on the novel hybrid structure of a nanoslit with embedded metallic nanoisland, which can be used for enhancing the field intensity at the transmitted side of a nanoslit.

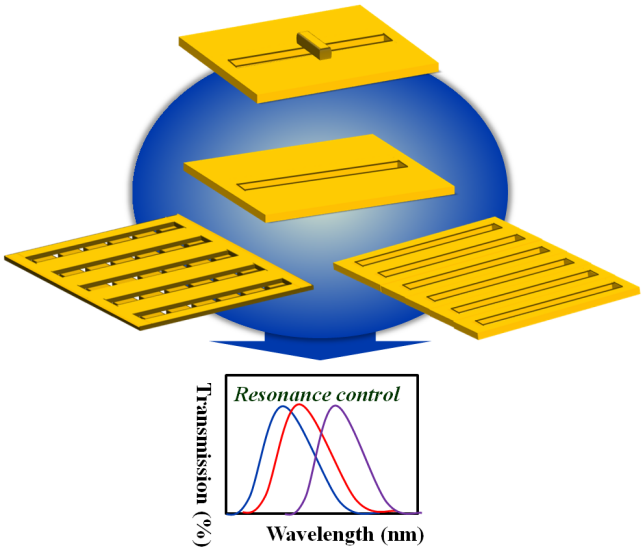

FIGURE 5. Various geometries extended from a nanoslit for the purpose of tuning resonance condition or optical characteristics.

III. FIELD ENHANCEMENT THROUGH A NANOSLIT BY THE USE OF METALLIC NANOISLANDS

Two main issues for a metallic nanoslit can be light intensity enhancement through a metallic nanoslit and tuning the resonance condition of metallic nanoslit. Recent researches have reported that resonance conditions through a metallic slit are influenced by resonant metallic nanoparticles placed within the structure or the array of metallic slits in terahertz and optical regime [70]–[74] as presented in Fig. 5. For example, Park *et al.* proposed that when a Pt nanoparticle is placed at the center position on the terahertz slot antenna, the electromagnetic coupling between the resonances supported by each of the two subwavelength metallic slits begins to unite and give rise to another mode [73]. Since they assumed that terahertz slot antenna is physically similar to a metallic slit, it provided the route to manipulate the resonant wavelength by controlling the dimension of a metallic slit. Meanwhile, resonant metallic nanoparticles placed within a metallic slit are attributed to the resonance condition as well. It is claimed that transmission spectra show how the size, orientation of the nanoparticles, and the period of the nanoslit array determine the maximum transmission wavelength, the magnitude of the transmission, and full width at half maximum (FWHM) of the resonance [74].

In these investigations, transmission of polarized light along the subwavelength slit was studied. But, these publications just provide the effect of resonance conditions with regard to the array of nanoslits, physical parameters of slit, or the position of a nanoparticle upon a slit. The mechanism of field enhancement when metallic nanoparticles or nanoislands are placed within a slit has not been unveiled. Hence, it is of interest to reveal the physics of field enhancement and propose a novel method to boost field intensity passing through a nanoslit.

In this Section, we propose the new pathway to enhance light intensity passing through a metallic nanoslit by embedding metallic rectangular nanoislands. We assume that the role of an embedded metallic nanoisland can be defined as a charge relocator and resonance shifter in a nanoslit for the intensity enhancement. To demonstrate experimentally, we measured the radiation intensity from the proposed structures by far-field scattering microscopy for the both polarization states of incident light at the specific wavelength. The intensity enhancement originates from induced accumulated charges from the embedded metallic rectangular nanoislands, which are excited from the incidence of both horizontal and vertical polarizations. In attempt to verify our model, the spectrum of proposed structures with respect to incident polarization is numerically analyzed. The degree of intensity enhancement can be determined by the number of embedded metallic rectangular nanoislands, which will be shown in experimental and numerical results. We also present that the resonance condition of a nanoslit could be tuned by the insertion of metallic rectangular nanoislands for the incidences of both horizontal and vertical polarizations.

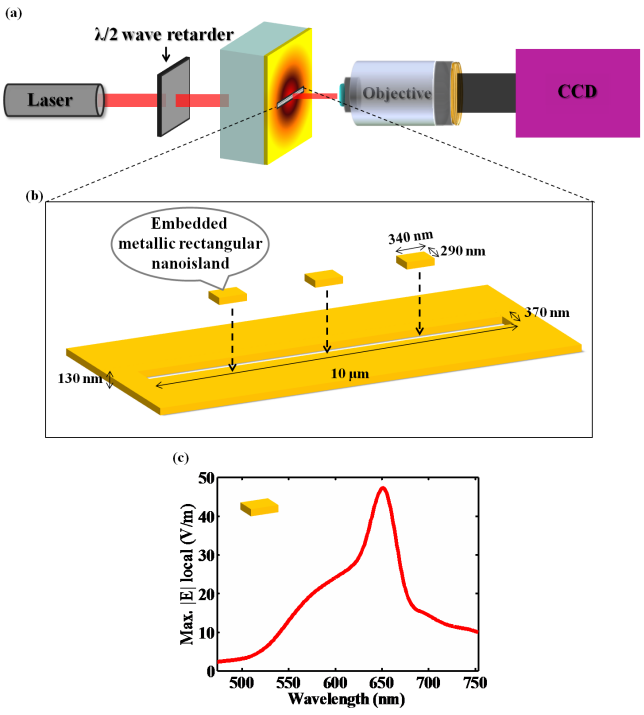

FIGURE 6. (a) Experimental setup to measure far-field radiation intensity from the proposed structures. (b) Schematic illustration of the proposed structure. (c) Numerical plot of maximum local electric field values on the top surface of a metallic rectangular nanoisland, changing the wavelength of incident light. The amplitude of incident electric field is 1(V/m).

A. EXPERIMENTAL CONFIGURATION AND RESULTS

Let us precisely describe the experimental configuration and the schematic of proposed structure. Figure 6(a) illustrates the experimental setup for the measurement of far-field light intensity. The proposed structure is illuminated from

the bottom by the laser with the free space wavelength of 660 nm (Newport, LQA660-110C) and the surface plasmon evanescent field intensity distribution was measured by the near-field scanning optical microscope (NSOM) (Nanonics, Multiview 4000). Far-field scattering microscopy equipped with a high numerical aperture (NA) objective (PlanApo, 100x, NA=0.85, Olympus Inc.) is used for far-field optical imaging. The transmitted light after interacting with the proposed structure is collected by an objective of 0.85 NA. We can acquire the microscopic images by a charge-coupled device (CCD) camera. Figure 6(b) provides the conceptual schematic diagram of the proposed structure. Typically, the transmitted light intensity through a nanoslit is weak. To overcome weak radiation from a nanoslit, we employ metallic rectangular nanoislands as a charge accumulator and relocator at a nanoslit for the enhancement of light intensity passing through a nanoslit. Metallic rectangular nanoislands are placed within a nanoslit ($10\,\mu m\,(x) \times 370\,nm\,(y)$). The dimension of a metallic rectangular nanoisland is developed from relevant references [17]. The size of the embedded metallic rectangular nanoisland is 340 nm (x) by 290 nm (y).

The thickness of thin film gold layer and gold rectangular nanoisland is 130nm and glass ($n = 1.5$) is used as a substrate. The thickness of metallic layer is thick enough to block the incident illuminated light. The thickness of a metallic rectangular nanoisland has been numerically optimized. In order to avoid the effect of thickness difference between thin film metal layer and metallic rectangular nanoisland, we establish the identical thickness of thin film metal layer with a metallic rectangular nanoisland. To identify the spectrum of a metallic rectangular nanoisland, we performed numerical calculations with three-dimensional finite difference time domain (FDTD) method, using the Palik parameters for the permittivity of Au [75], and assuming normal plane waves incident uniformly. The surrounding environment is assumed to be a vacuum and open boundary condition is used. The numerical plot of maximum electric field with respect to incident wavelength on the top surface of a metallic rectangular nanoisland, which is inserted inside a nanoslit, is exhibited in Fig. 6(c). As we ascertained in Fig. 6(c), the maximum field enhancement can be attained near the wavelength of 660 nm, which is equivalent to the wavelength of laser source. Accordingly, we expect to achieve considerable light enhancement through the proposed structure.

To experimentally demonstrate the functionalities of these proposed structures, we fabricated the proposed metallic structures. Electron beam evaporator (KVE-3004) is used for metal deposition onto the glass slide and the patterns are milled by focused ion beam machine. First of all, we investigate the case for the incidence of horizontally-polarized light with respect to a nanoslit in Fig. 7(a), one metallic rectangular nanoisland at the center of a nanoslit in Fig. 7(b), and three metallic rectangular nanoislands equally spaced at a nanoslit in Fig. 7(c). Figures 7(d)-7(f) show the far-field scattering intensity distributions of a nanoslit, one metallic rectangular nanoisland at the center of a nanoslit, and three

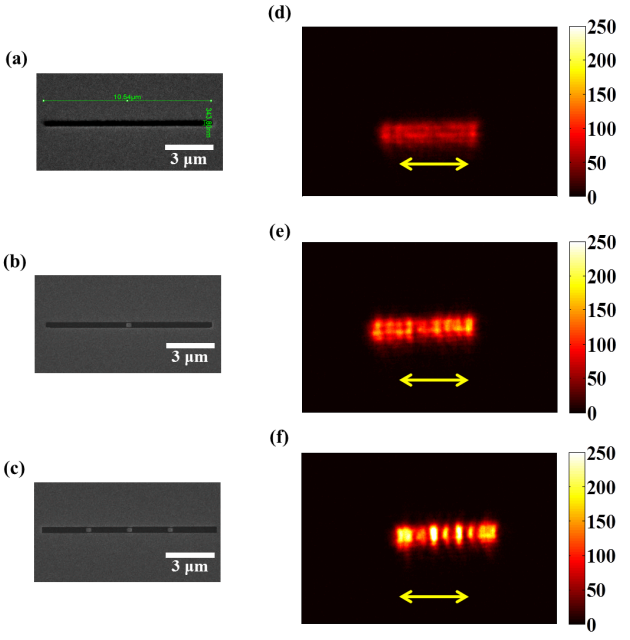

FIGURE 7. SEM pictures of (a) a nanoslit, (b) one metallic rectangular nanoisland placed at the center of a nanoslit, and (c) three metallic rectangular nanoislands equally spaced at a nanoslit. (d)-(f) Corresponding far-field scattering intensity profiles obtained from scattering microscopy, when illuminated by horizontally-polarized light.

metallic nanoislands equally spaced at a nanoslit, which are obtained from the scattering microscopy when illuminated by horizontally-polarized light. They show that when metallic rectangular nanoislands are embedded at a nanoslit, far-field scattering intensity is more enhanced than that of a simple nanoslit. In particular, Fig. 7(f) exhibits the strongest far-field scattering intensity, increased up to 2.5 times, which is stronger than the case of Fig. 7(d). It can be said that, within the scope of our experiments, as the number of embedded metallic rectangular nanoislands increases, the far-field scattering intensity gets stronger.

Meanwhile, when the proposed structures are illuminated by vertically-polarized light, far-field scattering intensity is also enhanced in comparison with that of a nanoslit as presented in Fig. 8. In this case, as the number of embedded metallic rectangular nanoislands increases, we achieve stronger far-field scattering intensity as well. Even though the physical principles are different with regard to the incident polarization state of light, far-field scattering intensity of the proposed structures exhibits almost similar profile regardless of the incident polarization states. In attempt to establish the role of embedded metallic nanoislands inside a nanoslit and examine the near-field profile, we measured the near-field intensity profile of proposed structures via near-field scanning optical microscopy (NSOM) as shown in the insets of Figs. 8(b) and 8(c).

Near-field intensity profiles show that radiation intensity at the interval between the edge of a metallic nanoslit and embedded metallic rectangular nanoisland is stronger than

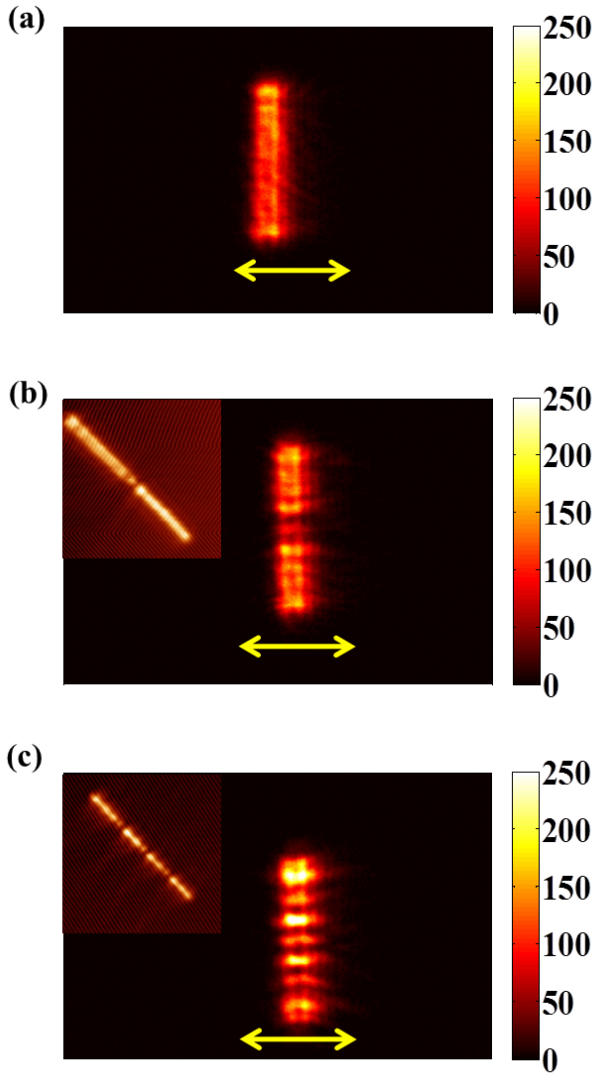

FIGURE 8. Far-field scattering intensity profiles of (a) a nanoslit, (b) one metallic nanoisland placed at the center of a nanoslit, and (c) three metallic nanoislands equally spaced at a nanoslit, obtained from scattering microscopy, when illuminated by light polarized vertically to the slit length direction. Inset images in (b) and (c) are corresponding near-field intensity profiles.

that above the embedded metallic rectangular nanoisland as shown in Figs. 8(b) and 8(c). Far-field intensity profiles show almost the identical profiles as near-field intensity profiles do. Even though this phenomenon cannot be directly explained by the localized plasmon effect of embedded metallic rectangular nanoislands, the increase of far-field scattering intensity would be attributed to near-field enhancement arisen from embedded metallic rectangular nanoislands by the correlation between NSOM image and far-field scattering image.

From these experimental results, we can suggest that the near- and far-field intensity passing through a nanoslit can be controlled by the number of embedded metallic rectangular nanoislands. However further study is needed to probe the effect of different shapes of noble metallic nanoislands embedded in a metallic nanoslit for the enhanced radiation.

B. THEORETICAL CONCEPTS AND NUMERICAL ANALYSIS

To verify and analyze experimental results, we numerically start to examine these proposed structures. Since a nanoslit is used as a reference structure, we should understand the fundamental characteristics of a nanoslit. Then, we try placing one and three metallic rectangular nanoislands inside a nanoslit to clarify not only the role of embedded metallic rectangular nanoislands but also the array effect of embedded metallic rectangular nanoislands. With these structures, we investigate the optical properties such as enhancement factor and resonance condition by changing the incident polarization state of light – horizontally-polarized light and vertically-polarized light.

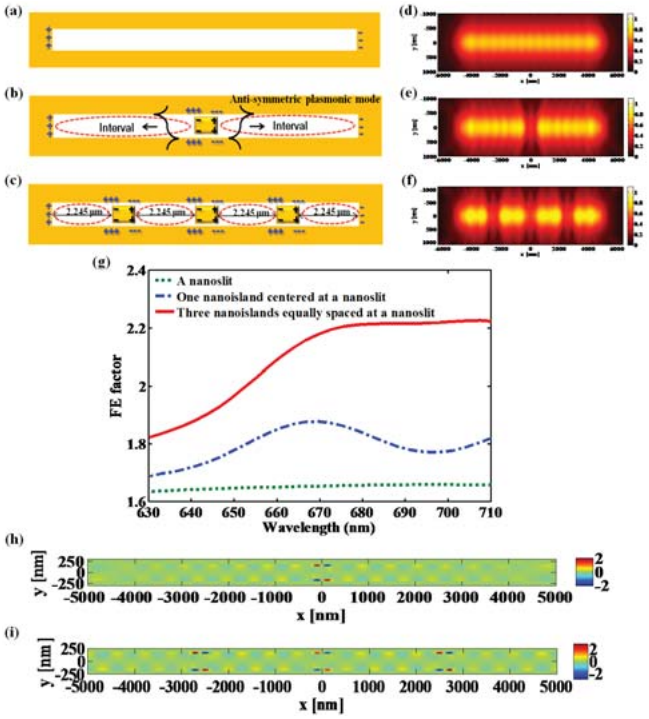

FIGURE 9. Charge redistribution model when illuminated by horizontally-polarized light and calculated far-field intensity distribution (a), (d) at a metallic nanoslit, (b), (e) one metallic rectangular nanoisland placed at the center of a nanoslit, (c), (f) three metallic rectangular nanoislands equally spaced at a nanoslit. (g) Their field enhancement factor is shown as a function of incident wavelength of horizontally-polarized light, which is calculated by numerical FDTD method. The amplitude of incident electric field is 1 (V/m). (h)-(i) Numerical E_y distribution at the middle depth of the nanoslit for the case of one embedded metallic rectangular nanoisland centered at a nanoslit, and three metallic rectangular nanoislands equally spaced at a nanoslit, respectively.

First of all, we would like to consider the case when a nanoslit (Fig. 9(a)) is illuminated by the incidence of horizontally-polarized light. In this case, the width of a nanoslit only allows two plasmonic TM modes and fundamental TE mode. However, TM modes cannot be generated inside the nanoslit due to the incident polarization, which means that only the fundamental TE mode can be allowed to transmit through a nanoslit. Since fundamental

TE mode has only the horizontal component of electric fields, which is normal to the left and right edges of a nanoslit, the fields cannot be considerably changed by the effect from those slit edges. Therefore, we can predict that the field profile inside a nanoslit does not show significant variation along the horizontal direction and the degree of electric field enhancement is not determined by the horizontal length of slit, when we ignore the role of SPPs [30]. Although these aspects cannot be directly adopted in near infrared and visible range, the spectrum of a nanoslit without nanoislands has almost the flat profile, which will be shown in the following paragraph (green dotted line of Fig. 9(g)). It indicates the effect from SPPs in a nanoslit is quite weak to change or enhance the overall spectrum of outgoing fields.

In an attempt to enhance this weak SPP excitation, we adopt the metallic rectangular nanoisland as a source of SPP excitation. Figure 9(b) describes the induced charge redistribution when one metallic rectangular nanoisland is placed at the center of a nanoslit. Charges of one metallic rectangular nanoisland are polarized by the incidence of horizontally-polarized light.

These polarized charges on this embedded metallic rectangular nanoisland attract opposite charges at the rim of a nanoslit near the embedded metallic rectangular nanoisland. Those charges are attributed to certain SPP source that horizontally propagates from the nanoisland, which is referred to as horizontally propagating *anti-symmetric plasmonic mode*. As compared to the case of a metallic nanoslit (Fig. 9(a)), *anti-symmetric plasmonic mode* is generated due to the symmetrically induced charges at the rim of a nanoslit resulted from the embedded metallic rectangular nanoisland. In other words, the amount of induced charges in the rim of a nanoslit near the embedded metallic rectangular nanoisland is increased. Additionally, in Fig. 9(c), three metallic rectangular nanoislands are equally spaced in a nanoslit. As the number of embedded metallic nanoislands is increased, the amount of induced charges is increased. From these effects, we can predict that field enhancement through the proposed structure can be achieved.

In order to prove our theoretical approaches, we numerically examine calculated far-field intensity distributions and total electric field integrated by effective area to measure the overall enhancement of electric field intensity. In Figs. 9(d) - 9(f), calculated far-field intensity distributions corresponding to each case are shown. Similar to the far-field experimental results, far-field intensity distribution is stronger as the number of embedded metallic nanoislands is increased. Likewise, low far-field scattering intensity at the position of embedded metallic nanoislands is numerically observed. It can be considered as the effect of dark plasmon mode from a metallic rectangular nanoisland [76]. To evaluate the degree of field enhancement via the proposed structure, we define FE factor as field enhancement factor, which is calculated by the electric field intensity at 100 nm above the proposed structures along the axis of propagation in x-y plane, then divided by the open area of proposed structure, when the magnitude of incident electric field is 1(V/m). Figure 9(g) reveals that FE factor is increased more in the proposed structure than that of a nanoslit over the calculated wavelength range. Placing metallic rectangular nanoisland inside a nanoslit lets the surface charge of a metallic nanoslit more polarized. Furthermore, FE factor of one metallic rectangular nanoisland placed at the center of a nanoslit is a little higher between 660 nm and 680 nm. The reason intuitively comes from the resonance condition of embedded metallic rectangular nanoisland. As we mentioned above, the metallic rectangular nanoisland has its own resonance near 660 nm. From these numerical results, we can recognize that localized surface plasmon resonance is obtained from the embedded metallic rectangular nanoisland and contributes to enhancement of FE factor. On the other hand, FE factor at a nanoslit without nanoislands inside it is almost constant as a function of incident wavelength. In addition, the number of embedded metallic rectangular nanoislands is increased from one to three in Figs. 9(b) and 9(c). We hypothesize that the more embedded metallic rectangular nanoislands are placed, the more extra charges are generated. We can confirm that Fig. 9(g) numerically shows the higher FE factor at the third structure than any other structures. In addition, we visualize the effect of SPPs from the embedded metallic rectangular nanoisland inside a nanoslit in Figs. 9(h) and 9(i). The y component of electric field distribution explicitly manifests the horizontally propagating *anti-symmetric plasmonic mode* generated from one metallic rectangular nanoisland centered at a nanoslit. In Fig. 9(i), we can identify three anti-symmetric plamsonic modes generated from each metallic nanoisland equally spaced at a nanoslit. These numerical results imply that the use of embedded metallic nanoislands is associated with the field intensity enhancement through a nanoslit in the incidence of horizontally-polarized light.

By the way, when vertically-polarized light is illuminated, we contemplate different optical phenomenon in the proposed structure. In opposition to the case for the incidence of horizontally-polarized light, only the fundamental TM mode is launched at the proposed structures for the normal incidence. Due to the finite length of nanoslit, this fundamental TM mode inside nanoslit has small modulation along horizontal direction and it makes weak resonant characteristics as shown in Fig. 10(g) (green dotted line). Similar to the case of horizontal incidence, placing the metallic rectangular nanoisland inside a nanoslit leads to generation of the horizontally propagating plasmonic modes. The charge redistribution model can be described as the horizontally propagating *symmetric plasmonic mode* in Figs. 10(b) and 10(c). In a same manner, the calculated far-field intensity distributions with respect to corresponding structures are shown in Figs. 10(d) - 10(f). Figure 10(g) indicates that FE factor periodically responds as a function of incident wavelength in a nanoslit. However, the FE factor between 630 nm and 690 nm is a little bit stronger in the case of one metallic rectangular nanoisland embedded in a nanoslit. In addition,

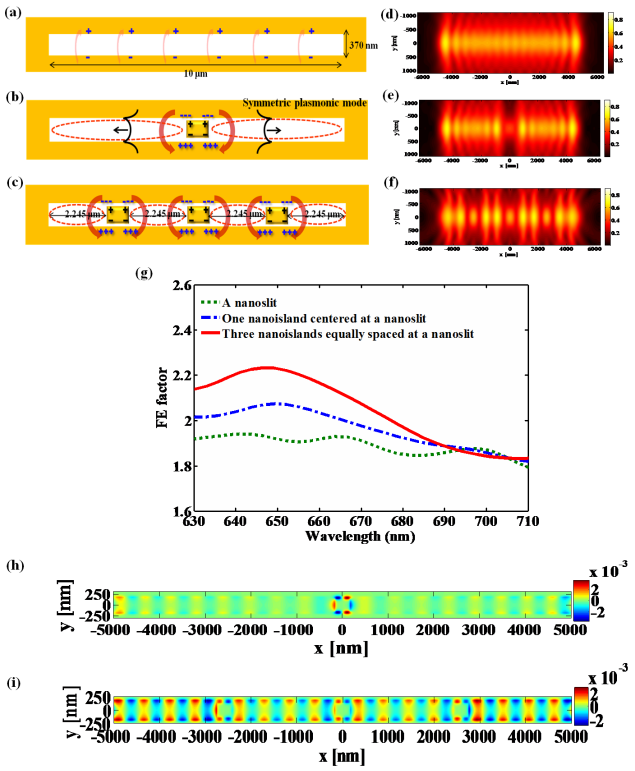

FIGURE 10. **Charge redistribution model when illuminated by vertically-polarized light and calculated far-field intensity distribution (a), (d) at a nanoslit, (b), (e) one metallic rectangular nanoisland placed at the center of a nanoslit, (c), (f) three metallic rectangular nanoislands equally spaced at a nanoslit. (g) Their FE factors are shown as a function of incident wavelength of vertically-polarized light, which is calculated by numerical FDTD method. The amplitude of incident electric field is 1 (V/m). (h)-(i) Numerical H_z distribution at the middle depth of the nanoslit for the case of one embedded metallic rectangular nanoisland centered at a nanoslit, and three metallic rectangular nanoislands equally spaced at a nanoslit, respectively.**

the peak position of FE factor is shifted to shorter wavelength. It can be said that both field enhancement and peak shift would result from the plasmonic resonance of the embedded metallic rectangular nanoisland.

The resonant wavelength of embedded metallic rectangular nanoisland is near 660 nm as previously presented in Fig. 6(c), which belongs to the range between 630 nm and 690 nm. That is why the incident wavelength of laser source belongs to the enhanced wavelength regime of FE factor. Although we cannot directly observe localized surface plasmon resonance (LSPR) from the embedded metallic nanoisland in a nanoslit on the incidence of vertically-polarized light, non-resonant effects from the nanogap formed between a nanoslit and a metallic rectangular nanoisland can also be used to further enhance field intensity [77]. A more physical interpretation attributes the enhanced fields to the build-up of opposite charges across the gap. In a similar manner, we recognize that when three metallic rectangular nanoislands equally spaced at a nanoslit are illuminated by vertically-polarized light, the strongest field enhancement is attained (Fig. 10(g)), like the case for the incidence of horizontally-polarized light. We also identify that the resonance is enhanced from the embedded metallic rectangular nanoisland centered at a nanoslit on the incidence of vertically-polarized light (as we called horizontally propagating *symmetric plasmonic mode*) in Figs. 10(h) - 10(i). Here, we show the z component of magnetic field distribution to verify the horizontally propagating symmetric plasmonic mode generated from a nanoisland, instead of y component electric field for filtering the incident field just in the case of vertically-polarized light. From this numerical analysis, we can identify that observed experimental results agree with the numerical results. Consequently, we can achieve intensity enhancement passing through a nanoslit, which involves embedded metallic rectangular nanoislands, accompanying with the shift of resonant wavelength arisen from embedded metallic rectangular nanoislands. Additionally, we figure out different physical principles with regard to the incident polarization state of light.

IV. CONCLUSIONS

In this invited paper, we overview the fundamentals of a nanoslit and deliver an extended research that includes the route for SPP excitation mechanism at a nanoslit accompanied with unidirectional launching. Furthermore, we propose a novel method to enhance light intensity passing through a nanoslit by employing embedded metallic nanoislands and demonstrate it via far-field scattering microscopy. The unique characteristics of the proposed structure are numerically explicated with regard to the polarization state of light. We observe that embedded metallic rectangular nanoisland can act as a charge relocator, accumulator, and resonance shifter in a nanoslit. These properties allow the proposed structure to achieve field intensity enhancement. Therefore, we believe that the proposed structure can be dedicated to the development of optical data storage [78], LSPR biosensors [79], and novel nano-photonics devices.

REFERENCES

[1] W. Barnes, A. Dereux, and T. Ebbesen, "Surface plasmon subwavelength optics," *Nature*, vol. 424, pp. 824–830, Aug. 2003.
[2] J. J. Burke, G. I. Stegeman, and T. Tamir, "Surface-polariton-like waves guided by thin, lossy metal films," *Phys. Rev. B*, vol. 33, no. 8, pp. 5186–5201, Apr. 1986.
[3] E. Ozbay, "Plasmonics: Merging photonics and electronics at nanoscale dimensions," *Science*, vol. 311, no. 5758, pp. 189–193, Jan. 2006.
[4] M. L. Brongersma and P. G. Kik, *Surface Plasmon Nanophotonics*. New York, NY, USA: Springer-Verlag, 2007.
[5] M. E. Stewart, C. R. Anderton, L. B. Thompson, J. Maria, S. K. Gray, J. A. Rogers, and R. G. Nuzzo, "Nanostructured plasmonic sensors," *Chem. Rev.*, vol. 108, no. 2, pp. 494–521, Feb. 2008.
[6] E. Hutter and J. H. Fendler, "Exploitation of localized surface plasmon resonance," *Adv. Mater.*, vol. 16, no. 19, pp. 1685–1706, Oct. 2004.
[7] L. V. Brown, H. Sobhani, J. B. Lassiter, P. Nordlander, and N. J. Halas, "Heterodimers: Plasmonic properties of mismatched nanoparticle pairs," *ACS Nano*, vol. 4, no. 2, pp. 819–832, Jan. 2010.
[8] T. Chung, S.-Y. Lee, E. Y. Song, H. Chun, and B. Lee, "Plasmonic nanostructures for nano-scale bio-sensing," *Sensors*, vol. 11, no. 11, pp. 10907–10929, Nov. 2011.
[9] N. Verellen, P. V. Dorpe, C. Huang, K. Lodewijks, G. A. E. Vandenbosch, L. Lagae, and V. V. Moshchalkov, "Plasmon line shaping using nanocrosses for high sensitivity localized surface plasmon resonance sensing," *Nano Lett.*, vol. 11, no. 2, pp. 391–397, Jan. 2011.

[10] F. Hao, C. L. Nehl, J. H. Hafner, and P. Nordlander, "Plasmon resonances of a gold nanostar," *Nano Lett.*, vol. 7, no. 3, pp. 729–732, Feb. 2007.

[11] T. W. Ebbesen, H. J. Lezec, H. F. Ghaemi, T. Thio, and P. A. Wolff, "Extraordinary optical transmission through sub-wavelength hole arrays," *Nature*, vol. 391, pp. 667–669, Feb. 1998.

[12] C. Genet and T. Ebbesen, "Light in tiny holes," *Nature*, vol. 445, pp. 39–46, Jan. 2007.

[13] W. Barnes, W. Murray, J. Dintinger, E. Devaux, and T. W. Ebbesen, "Surface plasmon polaritons and their role in the enhanced transmission of light through periodic arrays of subwavelength holes in a metal film," *Phys. Rev. Lett.*, vol. 92, no. 10, pp. 107401-1–107401-4, 2001.

[14] J. Coe, J. Heer, S. Teeters-Kennedy, H. Tian, and K. Rodriguez, "Extraordinary transmission of metal films with arrays of subwavelength holes," *Annu, Rev. Phys. Chem.*, vol. 59, pp. 179–202, Feb. 2008.

[15] N. Liu, T. Weiss, M. Mesch, L. Langguth, U. Eigenthaler, M. Hirscher, C. Sonnichsen, and H. Giessen, "Planar metamaterial analogue of electromagnetically induced transparency for plasmonic sensing," *Nano Lett.*, vol. 10, no. 10, pp. 1103–1107, Sep. 2010.

[16] S. Maier, P. Kik, H. Atwater, S. Meltzer, E. Harel, B. Koel, and A. Requicha, "Local detection of electromagnetic energy transport below the diffraction limit in metal nanoparticle plasmon waveguide," *Nat. Mater.*, vol. 2, no. 4, pp. 229–232, Mar. 2003.

[17] T. Chung, Y. Lim, I.-M. Lee, S.-Y. Lee, J. Choi, S. Roh, K.-Y. Kim, and B. Lee, "A compact light concentrator by the use of plasmonic faced folded nano-rods," *Opt. Exp.*, vol. 19, no. 21, pp. 20751–20760, Oct. 2011.

[18] D. F. P. Pile, T. Ogawa, D. K. Gramotnev, Y. Matsuzaki, K. C. Vernon, K. Yamaguchi, T. Okamoto, M. Haraguchi, and M. Fukui, "Two-dimensionally localized modes of a nanoscale gap plasmon waveguide," *Appl. Phys. Lett.*, vol. 87, no. 26, pp. 261114-1–261114-3, Dec. 2005.

[19] R. Bukasov and J. S. Shumaker-Parry, "Highly tunable infrared extinction properties of gold nanocrescents," *Nano Lett.*, vol. 7, no. 5, pp. 1113–1118, Apr. 2007.

[20] Y. Fu, Y. Liu, X. Zhou, Z. Xu, and F. Fang, "Experimental investigation of superfocusing of plasmonic lens with chirped circular nanoslits," *Opt. Exp.*, vol. 18, no. 4, pp. 3438–3443, Feb. 2010.

[21] L. Yin, V. Vlasko-Vlasov, J. Pearson, J. Hiller, J. Hua, U. Welp, D. Brown, and C. Kimball, "Subwavelength focusing and guiding of surface plasmons," *Nano Lett.*, vol. 5, no. 7, pp. 1399–1402, Jun. 2005.

[22] H. Lezec, A. Degiron, E. Devaux, R. Linke, L. Martin-Moreno, F. Garcia-Vidal, and T. Ebbesen, "Beaming light from a subwavelength aperture," *Science*, vol. 297, no. 5582, pp. 820–822, Jun. 2002.

[23] J. Yeh, J. Liu, C. Yeh, and C. Lee, "Physical origin of directional beaming emitted from a subwavelength slit," *Phys. Rev. B*, vol. 71, no. 4, pp. 041405-1–041405-4, 2005.

[24] D. Lin, C. Chang, Y. Chen, D. Yang, M. Lin, J. Yeh, J. Liu, C. Kuan, C. Yeh, and C. Lee, "Beaming light from a subwavelength metal slit surrounded by dielectric surface gratings," *Opt. Exp.*, vol. 14, no. 8, pp. 3503–3511, 2006.

[25] S. Kim, H. Kim, Y. Lim, and B. Lee, "Off-axis directional beaming of optical field diffracted by a single subwavelength metal slit with asymmetric dielectric surface gratings," *Appl. Phys. Lett.*, vol. 90, no. 5, pp. 051113-1–051113-3, Feb. 2007.

[26] D. Lin, T. Cheng, C. Chang, J. Yeh, J. Liu, C. Yeh, and C. Lee, "Directional light beaming control by a subwavelength asymmetric surface structure," *Opt. Exp.*, vol. 15, no. 5, pp. 2585–2591, Mar. 2007.

[27] S. Kim, Y. Lim, H. Kim, J. Park, and B. Lee, "Optical beam focusing by a single subwavelength metal slit surrounded by chirped dielectric surface gratings," *Appl. Phys. Lett.*, vol. 92, no. 1, pp. 013103-1–013013-3, Jan. 2008.

[28] B. Lee, S. Kim, H. Kim, and Y. Lim, "The use of plasmonics in light beaming and focusing," *Prog. Quantum Electron.*, vol. 34, no. 2, pp. 47–87, Mar. 2010.

[29] D. K. Gramotnev and S. I. Bozhevolnyi, "Plasmonics beyond the diffraction limit," *Nat. Photon.*, vol. 4, pp. 83–91, Jan. 2010.

[30] M. A. Seo, H. R. Park, S. M. Koo, D. J. Park, J. H. Kang, O. K. Suwal, S. S. Choi, P. C. M. Planken, G. S. Park, N. K. Park, Q. H. Park, and D. S. Kim, "Terahertz field enhancement by a metallic nano slit operating beyond the skin-depth limit," *Nat. Photon.*, vol. 3, pp. 152–156, Feb. 2009.

[31] J. W. Lee, T. H. Park, P. Nordlander, and D. M. Mittleman, "Terahertz transmission properties of an individual slit in a thin metallic plate," *Opt. Exp.*, vol. 17, pp. 12660–12667, Jul. 2009.

[32] J. S. White, G. Veronis, Z. Yu, E. S. Barnard, A. Chandran, S. Fan, and M. L. Brongersma, "Extraordinary optical absorption through subwavelength slits," *Opt. Lett.*, vol. 34, no. 5, pp. 686–688, Mar. 2009.

[33] A. Novitsky, M. Zalkovskij, R. Malureanu, P. U. Jepsen, and A. V. Lavrinenko, "Optical waveguide mode control by nanoslit-enhanced terahertz field," *Opt. Lett.*, vol. 37, no. 18, pp. 3903–3905, 2012.

[34] J. H. Kang, D. S. Kim, and Q.-H. Park, "Local capacitor model for plasmonic electric field enhancement," *Phys. Rev. Lett.*, vol. 102, no. 9, pp. 093906-1–093906-4, 2009.

[35] S. Collin, G. Vincent, R. Haidar, N. Bardou, S. Rommeluere, and J.-L. Pelouard, "Nearly perfect Fano transmission resonances through nanoslits drilled in a metallic membrane," *Phys. Rev. Lett.*, vol. 104, no. 2, pp. 027401-1–027401-4, 2010.

[36] J. Beermann, T. Sondergaard, S. M. Novikov, S. I. Bozhevolnyi, E. Devaux, and T. W. Ebbesen, "Field enhancement and extraordinary optical transmission by tapered periodic slits in gold films," *New J. Phys.*, vol. 13, no. 6, pp. 063029-1–063209-17, 2011.

[37] O. T. A. Janssen and H. P. Urbach, "Giant optical transmission of a subwavelength slit optimized using the magnetic field phase," *Phys. Rev. Lett.*, vol. 99, no. 4, pp. 043902-1–043902-3, Jul. 2007.

[38] F. J. Garcia-Vidal, H. J. Lezec, T. W. Ebbesen, and L. Martin-Moreno, "Multiple paths to enhance optical transmission through a single subwavelength slit," *Phys. Rev. Lett.*, vol. 90, no. 21, pp. 213901-1–213901-4, May 2003.

[39] C. M. Wang, H. I. Huang, C. C. Chao, J. Y. Chang, and Y. Sheng, "Transmission enhancement through a trench surrounded nano metallic slit by bump reflectors," *Opt. Exp.*, vol. 15, no. 6, pp. 3496–3501, 2007.

[40] J. W. Lee, M. A. Seo, D. J. Park, S. C. Jeoung, Q. H. Park, C. Lienau, and D. S. Kim, "Terahertz transparency at Fabry-Perot resonances of periodic slit arrays in a metal plate: Experiment and theory," *Opt. Exp.*, vol. 14, no. 26, pp. 12637–12643, Dec. 2006.

[41] A. I. Fernandez-Dominguez, A. Wiener, F. J. Garcia-Vidal, S. A. Maier, and J. B. Pendry, "Transformation-optics description of nonlocal effects in plasmonic nanostructures," *Phys. Rev. Lett.*, vol. 108, no. 10, pp. 106802-1–106802-5, Mar. 2012.

[42] K. J. Savage, M. M. Hawkeye, R. Esteban, A. G. Borisov, J. Aizpurua, and J. J. Baumberg, "Revealing the quantum regime in tunneling plasmonics," *Nature*, vol. 491, pp. 574–577, Nov. 2012.

[43] S.-Y. Lee, W. Lee, Y. Lee, J.-Y. Won, J. Kim, I.-M. Lee, and B. Lee, "Phase-controlled directional switching of surface plasmon polaritons via beam interference," *Laser Photon. Rev.*, vol. 7, no. 2, pp. 273–279, Mar. 2013.

[44] S.-Y. Lee, I.-M. Lee, J. Park, S. Oh, W. Lee, K.-Y. Kim, and B. Lee, "Role of magnetic induction currents in nanoslit excitation of surface plasmon polaritons," *Phys. Rev. Lett.*, vol. 108, no. 21, pp. 213907-1–213907-5, May 2012.

[45] A. Novitsky, A. M. Ivinskaya, M. Zalkovskij, R. Malureanu, P. U. Jepsen, and A. V. Lavrinenko, "Non-resonant terahertz field enhancement in periodically arranged nanoslits," *J. Appl. Phys.*, vol. 112, no. 7, pp. 074318-1–074318-10, Oct. 2012.

[46] M. Shalaby, H. Merbold, M. Peccianti, L. Razzari, G. Sharma, T. Ozaki, R. Morandotti, T. Feurer, A. Weber, L. Heyderman, B. Patterson, and H. Sigg, "Concurrent field enhancement and high transmission of THz radiation in nanoslit arrays," *Appl. Phys. Lett.*, vol. 99, no. 4, pp. 041110-1–041110-3, Jul. 2011.

[47] G. Zhao, "THz transmission properties of metallic slit array," *IEEE Trans. Terahertz Sci. Technol.*, vol. 3, no. 2, pp. 85–91, Feb. 2010.

[48] M. H. Lee, H. Gao, and T. W. Odom, "Refractive index sensing using quasi one-dimensional nanoslit arrays," *Nano Lett.*, vol. 9, no. 7, pp. 2584–2588, 2009.

[49] P. Lalanne, J. P. Hugonin, and J. C. Rodier, "Theory of surface plasmon generation at nanoslit apertures," *Phys. Rev. Lett.*, vol. 95, no. 26, pp. 263902-1–263902-4, Dec. 2005.

[50] J. A. Dionne, L. A. Sweatlock, H. A. Atwater, and A. Polman, "Planar metal plasmon waveguides: Frequency-dependent dispersion, propagation, localization, and loss beyond the free electron model," *Phys. Rev. B*, vol. 72, no. 7, pp. 075405-1–075405-11, 2005.

[51] J. Wuenschell and H. K. Kim, "Surface plasmon dynamics in an isolated metallic nanoslit," *Opt. Exp.*, vol. 14, no. 21, pp. 10000–10013, Oct. 2006.

[52] J. Chen, G. A. Smolyakov, S. R. J. Brueck, and K. J. Malloy, "Surface plasmon modes of finite, planar, metal-insulator-metal plasmonic waveguides," *Opt. Exp.*, vol. 16, no. 19, pp. 14902–14909, Sep. 2008.

[53] J. Park, K.-Y. Kim, I.-M. Lee, H. Na, S.-Y. Lee, and B. Lee, "Trapping light in plasmonic waveguides," *Opt. Exp.*, vol. 18, no. 2, pp. 598–623, Jan. 2010.
[54] M. A. Ordal, R. J. Bell, R. W. Alexander, Jr., L. L. Long, and M. R. Querry, "Optical properties of fourteen metals in the infrared and far infrared: Al, Co, Cu, Au, Fe, Pb, Mo, Ni, Pd, Pt, Ag, Ti, V, and W," *Appl. Opt.*, vol. 24, no. 24, pp. 4493–4499, 1985.
[55] Z. Han, L. Liu, and E. Forsberg, "Ultra-compact directional couplers and Mach–Zehnder interferometers employing surface plasmon polaritons," *Opt. Commun.*, vol. 259, no. 2, pp. 690–695, Mar. 2006.
[56] H. Kim, J. Park, S.-W. Cho, S.-Y. Lee, M. Kang, and B. Lee, "Synthesis and dynamic switching of surface plasmon vortices with plasmonic vortex lens," *Nano Lett.*, vol. 10, no. 2, pp. 529–536, Jan. 2010.
[57] S.-W. Cho, J. Park, S.-Y. Lee, H. Kim, and B. Lee, "Coupling of spin and angular momentum of light in plasmonic vortex," *Opt. Exp.*, vol. 20, no. 9, pp. 10083–10094, Apr. 2012.
[58] X.-P. Jin, X.-G. Huang, J. Tao, X.-S. Lin, and Q. Zhang, "A novel nanometeric plasmonic refractive index sensor," *IEEE Trans. Nanotechnol.*, vol. 9, no. 2, pp. 134–137, Mar. 2010.
[59] M. S. Jang and H. Atwater, "Plasmonic rainbow trapping structures for light localization and spectrum splitting," *Phys. Rev. Lett.*, vol. 107, no. 20, pp. 207401-1–207401-5, Nov. 2011.
[60] J. A. Dionne, K. Diest, L. A. Sweatlock, and H. A. Atwater, "PlasMOStor: A metal–oxide–Si field effect plasmonic modulator," *Nano Lett.*, vol. 9, no. 2, pp. 897–902, Jan. 2009.
[61] K. Y. Bliokh, Y. Gorodetski, V. Kleiner, and E. Hasman, "Coriolis effect in optics: Unified geometric phase and spin-hall effect," *Phys. Rev. Lett.*, vol. 101, no. 3, pp. 030404-1–030414-4, Jul. 2008.
[62] Y. Gorodetski, A. Niv, V. Kleiner, and E. Hasman, "Observation of the spin-based plasmonic effect in nanoscale structures," *Phys. Rev. Lett.*, vol. 101, no. 4, pp. 043903-1–043903-4, Jul. 2008.
[63] S. B. Raghunathan, C. H. Gan, T. van Dijk, B. Ea Kim, H. F. Schouten, W. Ubachs, P. Lalanne, and T. D. Visser, "Plasmon switching: Observation of dynamic surface plasmon steering by selective mode excitation in a sub-wavelength slit," *Opt. Exp.*, vol. 20, no. 14, pp. 15327–15335, Jul. 2012.
[64] Z. Liu, Y. Wang, J. Yao, H. Lee, W. Srituravanich, and X. Zhang, "Broad band two-dimensional manipulation of surface plasmons," *Nano Lett.*, vol. 9, no. 1, pp. 462–466, Dec. 2009.
[65] H. W. Kihm, K. G. Lee, and D. S. Kim J. H. Kang, and Q-H. Park, "Control of surface plasmon generation efficiency by slit-width tuning," *Appl. Phys. Lett.*, vol. 92, no. 5, pp. 051115-1–051115-3, Feb. 2008.
[66] G. Lévêque, O. J. F. Martin, and J. Weiner, "Transient behavior of surface plasmon polaritons scattered at a subwavelength groove," *Phys. Rev. B*, vol. 76, no. 15, pp. 155418-1–155418-5, Apr. 2007.
[67] B. Lee, I.-M. Lee, S. Kim, D.-H. Oh, and L. Hesselink, "Review on subwavelength confinement of light with plasmonics," *J. Modern Opt.*, vol. 57, no. 16, pp. 1479–1497, 2010.
[68] V. M. Shalaev, "Optical negative-index metamaterials," *Nat. Photon.*, vol. 1, no. 1, pp. 41–48, 2007.
[69] H. Kim and B. Lee, "Unidirectional surface plasmon polariton excitation on single slit with oblique backside illumination," *Plasmonics*, vol. 4, no. 2, pp. 153–159, Jul. 2009.
[70] Y. Pang, C. Genet, and T. W. Ebbesen, "Optical transmission through subwavelength slit apertures in metallic films," *Opt. Commun.*, vol. 280, no. 1, pp. 10–15, Dec. 2007.
[71] T. H. Isaac, J. Gomez Rivas, J. R. Sambles, W. L. Barnes, and E. Hendry, "Surface plasmon mediated transmission of subwavelength slits at THz frequencies," *Phys. Rev. B*, vol. 77, no. 11, pp. 113411-1–113411-4, Mar. 2008.
[72] Y. Xie, A. R. Zakharian, J. V. Moloney, and M. Mansuripur, "Transmission of light through slit apertures in metallic films," *Opt. Exp.*, vol. 12, no. 25, pp. 6106–6121, Dec. 2004.
[73] H.-R. Park, Y.-M. Bahk, K. J. Ahn, Q.-H. Park, D.-S. Kim, L. Martin-Moreno, F. J. Garcia-Vidal, and J. Bravo-Abad, "Controlling terzhertz radiation with nanoscale metal barriers embedded in nano slot antennas," *ACS Nano*, vol. 5, no. 10, pp. 8340–8345, Sep. 2011.
[74] M. J. Kofke, D. H. Waldeck, and G. C. Walker, "Composite nanoparticle nanoslit arrays: A novel platform for LSPR mediated subwavelength optical transmission," *Opt. Exp.*, vol. 18, no. 8, pp. 7705–7713, Apr. 2010.
[75] E. Palik, *Handbook of Optical Constant of Solids*. San Diego, CA, USA: Academic, 1985.
[76] A. M. Funston, C. Novo, T. J. Davis, and P. Mulvaney, "Plasmon coupling of gold nanorods at short distances and in different geometries," *Nano Lett.*, vol. 9, no. 4, pp. 1651–1658, Mar. 2009.
[77] J. A. Schuller, E. S. Barnard, W. Cai, Y. C. Jun, J. S. White, and M. L. Brongersma, "Plasmonics for extreme light concentration and manipulation," *Nature Mater.*, vol. 9, pp. 193–204, Feb. 2010.
[78] M. Mansuripur, A. R. Zakharian, A. Lesuffleur, S.-H. Oh, R. J. Jones, N. C. Lindquist, H. Im, A. Kobyakov, and J. V. Moloney, "Plasmonic nano-structures for optical data storage," *Opt. Exp.*, vol. 17, no. 16, pp. 14001–14014, Aug. 2009.
[79] W. Ma, J. Zhou, M. Yang, R. Tan, and H. Yuan, "A surface plasmon biosensor based on sub-wavelength metal slit arrays," *J. Phys. Conf. Ser.*, vol. 276, no. 1, pp. 012139-1–012139-6, 2011.

TAERIN CHUNG received the M.E. degree from the School of Electrical and Computer Engineering, Cornell University, Ithaca, NY, USA, in 2008. She is currently pursuing the Ph.D. degree with the School of Electrical Engineering, Seoul National University, Seoul, Korea.

Her current research interests include localized surface plasmon resonance and optical antenna.

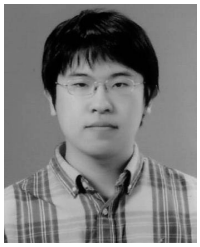

SEUNG-YEOL LEE is currently pursuing the Ph.D. degree with the School of Electrical Engineering, Seoul National University, Seoul, Korea.

His current research interests include surface plasmon resonance and waveguide devices.

HANSIK YUN received the M.S. degree from the Department of Chemical Engineering, Seoul National University, Seoul, Korea, in 2001, and the Ph.D. degree in electrical engineering from Seoul National University in 2013. He is currently a Post-Doctoral Researcher with the National Creative Research Center for Active Plasmonics Application Systems, Seoul National University.

His current research interest include surface plasmon resonance of metallic nanostructures.

SEONG-WOO CHO received the Ph.D. degree from the School of Electrical Engineering, Seoul National University, Seoul, Korea, in 2012. He is currently with Samsung Electronics, Geonggi-do, Korea. He was a Ph.D. course student with Seoul National University when this work was done.

YONGJUN LIM received the Ph.D. degree from the School of Electrical Engineering, Seoul National University, Seoul, Korea, in 2010. He is currently with Samsung Electronics, Geonggi-do, Korea. He was Post-Doctoral Researcher with Seoul National University when this work was done.

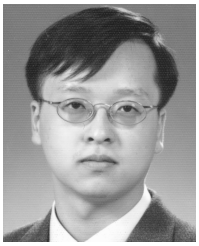

IL-MIN LEE received the Ph.D. degree from the School of Electrical Engineering, Seoul National University, Seoul, Korea, in 2009. He is currently a Post-Doctoral Scholar with National Creative Research Center for Active Plasmonics Application Systems, Seoul National University.

BYOUNGHO LEE (M'94–SM'00) received the Ph.D. degree in electrical engineering and computer science from the University of California at Berkeley, Berkeley, CA, USA, in 1993. In 1994, he joined the Faculty of the School of Electrical Engineering, Seoul National University, Seoul, Korea, where he is currently a Full Professor. He has been on the Board of Directors the Optical Society of America (OSA) and a member of the Strategic Planning Committee of OSA. His group has published more than 320 international journal papers and more than 570 international conference papers, including more than 100 invited talks. His current research interests include diffractive optics for nano-structures, surface plasmon polartions, and 3-D display. He is currently the Director of the National Creative Research Center for Active Plasmonics Application Systems funded by the Ministry of Science, ICT and Future Planning of Korea.

Dr. Lee is a fellow of SPIE, OSA, and a member of the Korean Academy of Science and Technology.